Applied Physics Letters PERSPECTIVE scitation.org/journal/apl

Impurities and defects in 4H silicon carbide

Cite as: Appl. Phys. Lett. **122**, 180501 (2023); doi: 10.1063/5.0145350
Submitted: 5 February 2023 · Accepted: 17 April 2023 ·
Published Online: 2 May 2023

Rong Wang,[1,2,a)] Yuanchao Huang,[1,2] Deren Yang,[1,2] and Xiaodong Pi[1,2,a)]

AFFILIATIONS

[1]State Key Laboratory of Silicon and Advanced Semiconductor Materials & School of Materials Science and Engineering, Zhejiang University, Hangzhou, Zhejiang 310027, China
[2]Institute of Advanced Semiconductors & Zhejiang Provincial Key Laboratory of Power Semiconductor Materials and Devices, Hangzhou Innovation Center, Zhejiang University, Hangzhou, Zhejiang 311200, China

[a)]**Authors to whom correspondence should be addressed:** rong_wang@zju.edu.cn and xdpi@zju.edu.cn

ABSTRACT

The widespread use of 4H silicon carbide (4H-SiC) is just around the corner since high-power electronics based on 4H-SiC are increasingly fabricated to enable the low-carbon development of the world. Quantum technologies are also intensively explored by scrutinizing 4H-SiC as a platform for wafer-scale integration of semiconductor and quantum technologies. Given the importance of impurities and defects for any semiconductor, comprehensive and insightful understanding of impurities and defects in 4H-SiC is imperative. In this Perspective, we summarize recent experimental and theoretical advances in researches on impurities and defects in 4H-SiC after briefly reviewing the history of 4H-SiC. Impurity engineering and defect engineering for the realization of the full potential of 4H-SiC are also discussed. Challenges for the study on impurities and defects in 4H-SiC are finally outlined.

I. INTRODUCTION

The low-carbon development of the world needs high-performance power semiconductor devices to support the generation, transportation, and utilization of electricity. As a wide-bandgap semiconductor, silicon carbide (SiC) has recently gained great popularity for the fabrication of power semiconductor devices due to its superior properties, such as high breakdown electric field strength, high carrier mobility, and high thermal conductivity.[1,2] SiC also plays a critical role in the development of quantum technologies, where the coherent manipulation of a single spin state has been demonstrated at room temperature.[3,4] The application of SiC has also expanded to photoconductive switches, radiation detectors, optical detectors, and two-dimensional (2D)-material sciences.[5–8] According to the stacking orders of the Si-C bilayers, SiC has more than 200 polymorphs, among which 3C-, 4H-, and 6H-SiC are the most common polymorphs. First-principles calculations indicate that the conduction-band minimum (CBM) tends to float in interstitial channels of SiC.[9] The different stacking sequences of Si-C bilayers in different SiC polymorphs give rise to the different shapes of the interstitial channels and, thus, the different CBM characteristics.[9] This results in the different band structures of different SiC polymorphs.[9] Owing to the highest Baliga's figure-of-merit of 4H-SiC,[10] the single-crystal growth and homoepitaxy of 4H-SiC followed by the fabrication of 4H-SiC power devices have been the most intensively investigated. The incoming widespread use of 4H-SiC in power electronics should render a mature infrastructure of 4H-SiC, which may facilitate the large-scale deployment of quantum devices, photoconductive switches, radiation detectors, optical detectors, and 2D-material sciences based on 4H-SiC.

Impurities and defects have been found to significantly affect the electrical, thermal, and optical properties of semiconductors.[11–13] Intentional doping is traditionally used to incorporate impurities and tune the electrical conductivity of 4H-SiC. For instance, nitrogen (N) and aluminum (Al) are intentionally incorporated into 4H-SiC to realize *n*-type and *p*-type doping of 4H-SiC, respectively,[1] while unintentional incorporated impurities and defects usually exert detrimental effect on the properties of 4H-SiC, degrading the performance and reliability of semiconductor devices based on 4H-SiC. For example, point defects such as carbon vacancies (V_C) have been found to reduce the minority-carrier lifetime of 4H-SiC.[14] Dislocations have been found to reduce the minority-carrier lifetime of 4H-SiC, increase the leakage current, and bring reliability issues of power devices based on 4H-SiC.[14,15] More significantly, impurity engineering and defect engineering, such as codoping, defect passivation, defect-complex design, and excitation-state manipulation (e.g., illumination, irradiation, and charge injection), have been widely used to tailor the detrimental defect states and exploit novel material properties.[16–20] Therefore, comprehensive and insightful understanding on impurities and defects

of 4H-SiC is imperative to explore the full potential of increasingly important 4H-SiC.

In this Perspective, we summarize experimental and theoretical researches on impurities and defects in 4H-SiC. A prospect about the development trend and challenges of the impurity engineering and defect engineering of 4H-SiC are presented. First, we introduce the doping of 4H-SiC for applications including modern electronics and quantum information technologies. The impurity engineering and defect engineering toward high-performance *p*-type 4H-SiC are proposed by analyzing the challenges of the *p*-type doping of 4H-SiC. The geometric configurations, electronic structures, and optical properties of defects, including point defects, dislocations, stacking faults, and other three-dimensional defects, are then presented. The defect control and defect engineering of point defects, dislocations, and stacking faults are proposed toward high-quality 4H-SiC. Finally, challenges of the impurity engineering and defect engineering of 4H-SiC are outlined to push forward the application of 4H-SiC in high-power and high-frequency electronics and explore the full potential of 4H-SiC in quantum technologies, photoconductive switches, radiation/optical detectors, and 2D-material sciences.

II. DOPING AND IMPURITY ENGINEERING OF 4H-SiC

A. Doping and impurity engineering of 4H-SiC used in modern electronics

For 4H-SiC used in high-power and high-frequency electronics, it is critical to control the electronic conductivities by intentional doping.[21] *n*-Type and *p*-type doping of 4H-SiC can be achieved by the substitution of Si (or C) by group-V and group-III impurities, respectively. There exist cubit lattice sites (*k*-sites) and hexagonal lattice sites (*h*-sites) for Si and C in 4H-SiC.[22] The ionization energy of a substitutional donor at the *k* sites (D_k) is 1.88 times higher than that at the *h* site (D_h), and the ionization energies of a substitutional acceptor at the *k* site and the *h* site are almost the same.[23] The doping of 4H-SiC used in high-power and high-frequency electronics is summarized in Fig. 1. Among group-V impurities, nitrogen (N) has the lowest ionization energy by substituting carbon atoms (N_C). First-principles calculations and experimental researches indicate that the ionization energies of N_C at the *k* site and the *h* site are in the ranges of 0.10–0.12 and 0.05–0.06 eV, respectively.[23–25] The gives rise to almost 100% ionization of N_C. The N doping of 4H-SiC is the most well-developed. The concentration of N dopants can be accurately controlled in the range of $10^{14}\,cm^{-3}$–$10^{20}\,cm^{-3}$,[26] which enables N-doped 4H-SiC a great success in applications such as electrical vehicles and photovoltaic inverters.

p-Type 4H-SiC has attractive applications in ultra-high-power electronics for high-voltage grids and high-speed trains. However, the development of *p*-type doping prominently lags behind the *n*-type doping of 4H-SiC. Aluminum (Al) has the lowest ionization energy among group-III atoms by substituting Si atoms.[27] However, both experimental researches and first-principles calculations have found that the $(0/-)$ transition energy of Al_{Si} is 0.20–0.23 eV in 4H-SiC, which gives rise to incomplete ionization of Al_{Si} in 4H-SiC.[23,27–29] As the concentration of Al increases from 10^{14} to $10^{19}\,cm^{-3}$, the incomplete ionization ratio of Al_{Si} decreases from 90% to 5% at room temperature.[30] When the concentration of Al_{Si} is higher than $10^{20}\,cm^{-3}$, the incomplete ionization ratio of Al_{Si} increases instead because of the variable range hopping (VRH) conduction mechanism.[30,31] Boron (B)

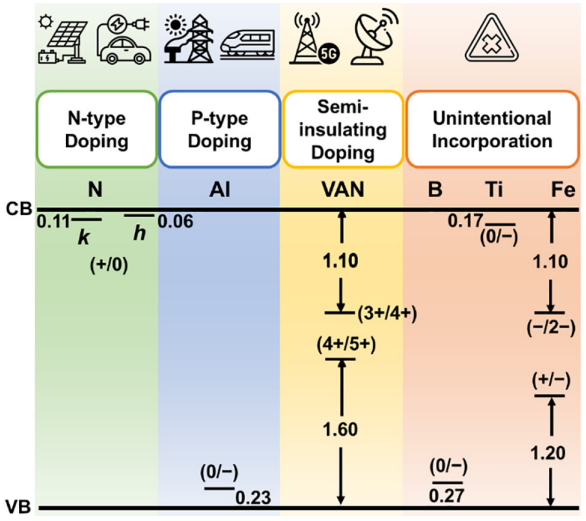

FIG. 1. Doping of 4H-SiC in high-power and high-frequency electronics. The charge transition energies of dopants and unintentional incorporated impurities are labeled in the figure.[23,29,40–42]

might be a potential candidate for the *p*-type doping of 4H-SiC, with the $(0/-)$ transition energy level of B_{Si} being 0.27 eV.[32] However, B has the problem of abnormal diffusion in 4H-SiC.[33] Therefore, the impurity engineering in *p*-type 4H-SiC mainly focuses on reducing the resistivity of Al-doped 4H-SiC.

The high ionization energy of Al in 4H-SiC is the main challenge of the *p*-type doping of 4H-SiC. As shown in Fig. 2(a), the defect state of Al_{Si} is derived from the valence band maximum (VBM) of 4H-SiC that moves upward in energy. The defect state is double degenerate (*e* state), which is occupied by three electrons. In order to push the defect state of Al_{Si} downward the VBM of 4H-SiC, a defect with the empty *e* state (X) is desired to contribute the repulsion between these defect states with the same symmetry and maintain the ability to accept the electron from the VBM of 4H-SiC. First-principles calculations indicate that group-IVB impurities, especially titanium (Ti), are attractive to reduce the ionization energy of Al_{Si}.[29] From the point of

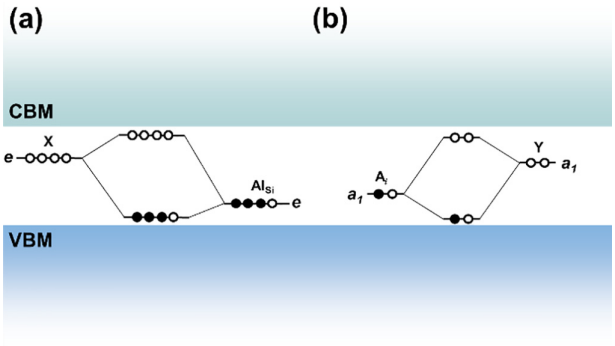

FIG. 2. Schematic illustration of (a) level repulsion to reduce the $(0/-)$ transition energy of Al_{Si} in Al-doped 4H-SiC, (b) design of an interstitial acceptor (A_i), and the level repulsion in A_i-doped 4H-SiC. The closed and open circles represent electrons and holes, respectively.

view of increasing the effective incorporation of Al species, the *p*-type doping of 4H-SiC can also be improved by doping on the Si face of 4H-SiC and tuning the C-rich growth conditions, which provides more incorporation sites of Al species.[34]

Interstitials that introduce a semi-occupied a_1 state derived from the CBM of 4H-SiC could also be engineered toward *p*-type doping of 4H-SiC. Potential candidates for the interstitial acceptors include group-I dopants. As shown in Fig. 2(b), even the interstitial acceptor (A_i) has a deep acceptor state, and the defect state can be lowered by designing defect-state-repulsion between the defect states of A_i and another impurity or defect (Y) with an empty a_1 state. We note that the impurity engineering of codoping is convenient in the solution growth and chemical vapor deposition (CVD) of 4H-SiC by continuously introducing doping sources. During the physical vapor transport (PVT) growth of 4H-SiC, careful design of the introduction of doping sources and the differences in the sublimation temperatures between growth and doping species are required.

In addition to the incomplete ionization, the compensation of intrinsic defects also degrades the resistivity of Al-doped 4H-SiC. First-principles calculations have indicated that V_C^{2+} leads to Fermi level pinning and thus compensates the *p*-type doping of 4H-SiC.[35] During the growth and *p*-type doping of 4H-SiC, the C-rich condition is also preferred from the point of view of reducing the V_C concentration, relieving the Fermi-level pinning and decreasing the resistivity of *p*-type 4H-SiC. The defect engineering to eliminate or relieve the detrimental effect of V_C needs to be carried out as post-growth treatments of *p*-type 4H-SiC. The generation and diffusion of carbon interstitials (C_i) are capable of passivating V_C. For example, C ion implantation followed by thermal annealing can reduce the concentration of V_C and reduce the resistivity of *p*-type 4H-SiC.[36,37] Furthermore, hydrogen (H) passivation of native defects has been widely established in semiconductors such as silicon and gallium nitrides.[20,38] First-principles defect calculations indicate that the V_C-H_x ($x = 1$–4) complexes have higher formation energy than individual V_C, indicating that H cannot passivate V_C in 4H-SiC under thermodynamic equilibrium conditions.[25] Therefore, non-thermodynamic equilibrium conditions such as light illumination, charge injection, and H ion implantation should be carefully designed for the H passivation of V_C^{2+} and reduction of the resistivity of *p*-type 4H-SiC.

When 4H-SiC is used as the substrate of group-III nitrides in high-frequency electronics, semi-insulating (SI) 4H-SiC with the resistivity higher than 10^9 Ω·cm is highly desired.[39] Since the high-temperature growth of 4H-SiC is usually carried out in a graphite-contained environment, impurities such as B, iron (Fe), and Ti escaped from graphite components are incorporated into SI 4H-SiC. The defect states of these unintentional incorporated impurities might degrade the SI conductivity of 4H-SiC.[32,40,41] N can also be incorporated into SI 4H-SiC as a result of imperfect vacuum control. Vanadium (in order to distinguish vanadium from vacancies, vanadium is abbreviated as "VAN" in this Perspective) has been found to create mid-gap defect states,[42] which facilitates the SI conductivity and overcomes the unintentional background doping of 4H-SiC.[43] At the early-stage development of 4H-SiC, VAN-doped SI 4H-SiC substrates were commonly used as the substrate of microwave devices. However, the trapping of electrons by VAN in SI 4H-SiC substrates gives rise to the parasitic effect of microwave devices.[44] Since the development of the vacuum control of the growth chamber and the purification of graphite components have been better controlled during the PVT growth of 4H-SiC, the high-purity semi-insulating (HPSI) 4H-SiC with impurity concentrations lower than 10^{15} cm^{-3} has been successfully industrialized.[45,46] In addition to the application of SI 4H-SiC in high-frequency electronics, SI 4H-SiC has been emerged as an ideal materials for photoconductive switches.[47] High-performance photoconductive switches based on HPSI and VAN-doped 4H-SiC triggered by 355-nm and 532-nm lasers have been successfully demonstrated, respectively.[48–50] 355-nm lasers are usually generated by tripler of 1064-nm Nd:YAG lasers. From the point of view of minimizing energy loss during the tripler, photoconductive switches based on VAN-doped SI 4H-SiC triggered by Nd:YAG 532-nm lasers are more attractive.[50] Furthermore, impurity engineering of HPSI 4H-SiC, which induces mid-gap states, facilitates the triggering of different-wavelength lasers and maintains the SI conductivity of 4H-SiC, which would benefit the application of photoconductive switches triggered by different-wavelength lasers.

B. Doping of 4H-SiC for quantum technologies

SiC has emerged as an ideal platform for the wafer-scale integration of quantum technologies owing to the feasible optical and electrical control of qubits, which rely on quantum emission from fluorescent isolated impurity or point defect in SiC.[51] Coherent control of electron spin of impurities and point defects has been realized in 3C-, 4H-, and 6H-SiC.[4] 3C-SiC is heteroepitaxially grown on silicon (Si) substrates, the lattice mismatch, and thermal-expansion-coefficient mismatch between 3C-SiC and Si results in internal stress in 3C-SiC, which degrades the nonlinear optical property of 3C-SiC. Compared with 4H-SiC, the impurity and point-defect quantum qubits are less studied in 6H-SiC because the technical maturity for the growth of 6H-SiC is lower. The three inequivalent sub-lattice sites in 6H-SiC raise the difficulty in identifying defect configurations. In this Perspective, we concentrate on the doping and point-defect design of 4H-SiC for quantum technologies. The most typical characteristic in the quantum properties of color centers is the zero-phonon line (ZPL). Table I tabulates the configurations, ZPL values, and quantum emission wavelengths of color centers in 4H-SiC.[2] It is clear that the values of the ZPL of most color centers are located in the near-infrared region, which is desirable for the long-distance telecommunications. We note that the optically active color centers are in the non-thermal equilibrium states of impurities in 4H-SiC. This indicates that the generation of these color centers requires non-thermal equilibrium treatments, such as ion implantation, high-energy particle (e.g., electron, proton, or neutron) irradiation, and high-pressure engineering.[52–54]

III. DEFECTS AND DEFECT ENGINEERING OF 4H-SiC

As shown in Fig. 3, defects in 4H-SiC can be classified by the dimension of defects. In this section, we summarize the effect of different defects on the electronic and optical properties of 4H-SiC. By pointing out the challenges of defect control in 4H-SiC, we propose possible approaches to reduce the defect density and tailor the detrimental defect states in 4H-SiC.

A. Zero-dimensional defects

Point defects such as vacancies, interstitials, and antisites, as well as the complexes of impurities and point defects belong to

TABLE I. Configurations, ZPL values, and quantum emission wavelengths of color centers in 4H-SiC.[55–63]

Color centers	Defect configuration and charge state	Zero-phonon line (eV)	Quantum emission wavelength (nm)
Nitrogen-vacancy (NV)[55,56]	$(N_C^h V_{Si}^h)^{1-}$	0.998	1242.5
	$(N_C^h V_{Si}^k)^{1-}$	1.014	1222.9
	$(N_C^k V_{Si}^h)^{1-}$	1.051	1179.8
	$(N_C^k V_{Si}^k)^{1-}$	0.999	1241.2
Vanadium (VAN)[57]	$(VAN_{Si}^h)^0$	0.929	1334.8
	$(VAN_{Si}^k)^0$	0.969	1279. 7
Chromium (Cr)[58]	$(Cr_{Si}^h)^{4+}$	1.190	1042.0
	$(Cr_{Si}^k)^{4+}$	1.158	1070.8
Molybdenum (Mo)[59]	$(Mo_{Si}^h)^{1+}$	1.152	1076.4
Niobium (Nb)[60]	$(Nb_{Si}^h V_C^h)^0$	1.383	896.6
Silicon vacancy (V_{Si})[61]	$(V_{Si}^h)^{1-}$	1.438	862.3
	$(V_{Si}^k)^{1-}$	1.352	917.2
Divacancy (VV)[52]	$(V_C^h V_{Si}^h)^0$	1.095	1132.4
	$(V_C^h V_{Si}^k)^0$	1.119	1108.1
	$(V_C^k V_{Si}^h)^0$	1.150	1078.3
	$(V_C^k V_{Si}^k)^0$	1.096	1131.4
Carbon antisite-carbon vacancy (CAV)[63]	$(V_C^h C_{Si}^h)^0$	0.81	1530.9
	$(V_C^h C_{Si}^k)^0$	0.83	1494.0
	$(V_C^k C_{Si}^h)^0$	0.95	1305.3
	$(V_C^k C_{Si}^k)^0$	0.86	1441.9

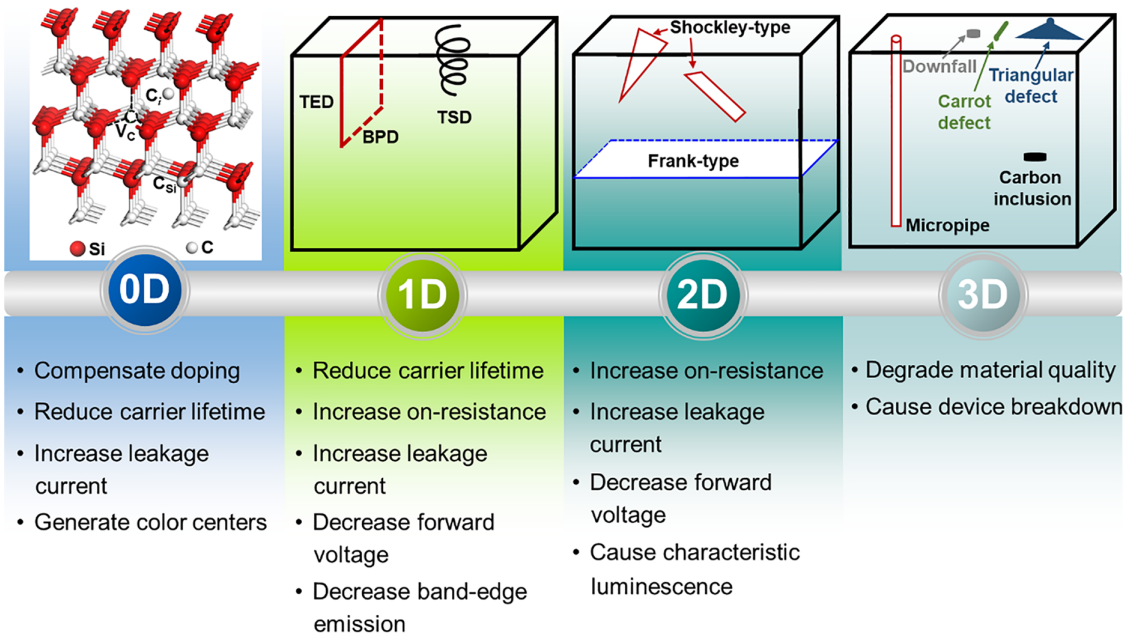

FIG. 3. Classifications and illustrations of defects in 4H-SiC. The effects of defects on the properties of 4H-SiC and the performance of power devices based on 4H-SiC are shown in the lower panel.

zero-dimensional (0D) defects. First-principles calculations indicate that positively charged carbon vacancy (V_C) and neutral antisites (Si_C) are dominant point defects in *p*-type and *n*-type 4H-SiC, respectively,[23] which have been verified by various experimental measurements.[14,64] V_C^{2+} has been found to compensate the *p*-type doping and reduce the carrier lifetime of 4H-SiC.[35,65] In bipolar devices based on 4H-SiC, the long carrier lifetime of a lightly N-doped voltage-blocking epitaxial layer is highly desired to maintain the injection of minority carriers.[66] However, the acceptor transition level of V_C ($Z_{1/2}$) has been found to reduce the minority lifetime of lightly N-doped 4H-SiC.[14,67] It has been found that the Z_1 center and Z_2 center originate from V_C locating at the *h*-sites and *k*-sites, respectively.[68,69] Furthermore, defect levels induced by V_C have also been found to participate in the phonon-assisted tunneling current of power devices based on 4H-SiC.[70,71] Therefore, defect engineering to eliminate the defect levels of V_C is imperative for the application of 4H-SiC in power electronics. As discussed earlier, the improvement of the minority-carrier lifetime relies on reducing the concentration of V_C during the growth of 4H-SiC. Defect engineering approaches to eliminate or relieve the detrimental effect of V_C also need to be carried out as post-growth treatments to improve the carrier lifetime of 4H-SiC. Meanwhile, numerical simulations indicate that the surface recombination and carrier recombination in the 4H-SiC substrate exert significant effect on the carrier lifetime of 4H-SiC homoepitaxial layers.[72] Therefore, these minority-carrier recombination paths need to be taken into account in the defect engineering to improve the minority-carrier lifetime of 4H-SiC homoepitaxial layers and enhance the performance of high-power devices based on 4H-SiC.

Owing to its strong radiation resistance, semiconductor devices based on 4H-SiC hold great promise in extreme-environment applications, where 4H-SiC materials are often subjected to the irradiation of electrons, protons, heavy ions, and neutrons.[73] When the energies of these particles exceed the threshold displacement energy of Si or C in 4H-SiC, irradiation-induced damages are generated. It has been found that irradiation-induced damages are mainly deep-level point defects, including V_C, silicon vacancies (V_{Si}), divacancies (VV), carbon interstitials (C_i), and carbon antisite-carbon vacancy (CAV) complexes.[74–79] Although the irradiation-induced displacement damages degrade the properties of 4H-SiC, thus the performance of 4H-SiC based devices, electron irradiation has been adopted as an attractive approach to tune the SI conductivity of 4H-SiC by the introduction of low-energy irradiation-induced V_C.[80]

Furthermore, V_{Si}, VV, and CAV complexes are highly desired for 4H-SiC used in quantum technologies (Table I).[61–63] Again, careful design of non-thermodynamic equilibrium processing technologies (e.g., ion implantation, ultra-fast laser writing, high-pressure treatments, and high-energy particle irradiation) should be conducted to guarantee the uniform distribution of these defects.[81–83] Since V_C is inevitably generated during the growth and high-energy particle irradition,[84,85] V_C might disturb the uniform distribution of color centers, degrade the optical fine structure of quantum emitters, and cause spin decoherence of optically active qubits, which needs further investigation.

B. One-dimensional defects

Dislocations are one-dimensional (1D) defects in 4H-SiC. According to the Burgers vectors, dislocations in 4H-SiC can be classified into threading edge dislocations (TEDs), threading screw dislocations (TSDs), threading mixed dislocations (TMDs), and basal plane dislocations (BPDs). Dislocations have been found to reduce the carrier lifetime, increase the leakage current, and reduce the forward voltage of power devices based on 4H-SiC.[86,87] A detailed review on the configurations, evolutions, and effects of dislocations in 4H-SiC can be found in Ref. 15. Since the carrier recombination at dislocations weakens the band edge emission of 4H-SiC and induces characteristic luminescence of 4H-SiC,[88,89] dislocations might degrade the quantum emission of color centers in 4H-SiC. On the other hand, first-principles calculations have revealed that screw dislocations in semiconductors serve as a 1D topological defect that would account for the superconducting transition.[90] Therefore, the manipulation of dislocations, especially screw dislocations, holds promise in broaden the application of 4H-SiC in quantum technologies.

Dislocations are generated during the single-crystal growth, wafer processing, and homoepitaxy of 4H-SiC.[15,91] Reducing the dislocation density, especially the densities of TMDs, TSDs, and BPDs, is a long-standing issue in the development of 4H-SiC with improved electrical and thermal conductivities, increased carrier lifetime, enhanced device performance, and bipolar reliability. Since BPDs lead to the bipolar degradation of bipolar devices based on 4H-SiC,[92] the conversion from BPDs to TEDs has been pursued during the homoepitaxy of 4H-SiC.[93] However, TEDs are also found to increase the leakage current of 4H-SiC, although the effect of TEDs is less serious than those of TSDs and TMDs.[87] Reducing the total density of dislocations is critical to optimizing the quality of 4H-SiC and enhancing the performance of semiconductor devices based on 4H-SiC. The repeated ***a***-face (RAF) growth method and hybrid growth method combining solution growth and PVT growth have been demonstrated to be capable of reducing the density of threading dislocations in 4H-SiC single crystals.[94,95] Herein, we propose that the reduction of the total dislocation densities of 4H-SiC substrates and homoepitaxial layers might be realized by designing a buffer layer that promotes the conversion from TSDs (or TEDs) to stacking faults (or BPDs). As shown in Fig. 4, the conversion of TDs to basal plane defects (stacking faults and BPDs) can be assisted by macrosteps along the step-flow direction. The transition has been successfully realized in the solution growth of 4H-SiC single crystals.[96,97] In the well-developed PVT and CVD growth of 4H-SiC, it is imperative to enable growth conditions to realize the step-flow growth and maintain low growth speed at the initial growth stage to promote the conversion of TDs and leave the converted basal plane defects in the buffer layer.

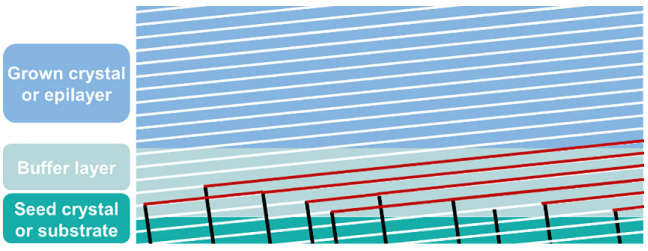

FIG. 4. Schematic diagram showing the conversion of TDs in the buffer layer of a 4H-SiC epilayer (or single crystal) grown on a 4H-SiC substrate (or seed crystal). The growth steps, TDs, and basal plane defects are denoted by white, black, and red lines, respectively.

Dopants such as N and VAN have been found to change the electronic properties and kinetics of dislocations in 4H-SiC.[98–100] For dislocations already existing in 4H-SiC, it would be potential to manipulate the properties of dislocations by intentional doping to relieve the detrimental effect of dislocations. Based on the fact that dislocations are often decorated by point defects (or impurities), the interaction between dislocations and high-energy particle irradiation-induced point defects has been found to change the defect-level positions of dislocations in gallium nitrides.[101,102] Similarly, the high-energy particle irradiation would be utilized as a potential defect-engineering approach to tune the defect-level position of dislocations in 4H-SiC and optimize the dislocation behaviors in semiconductor devices based on 4H-SiC.

C. Two-dimensional defects

Stacking faults (SFs), which can be classified into Frank-type and Shockley-type SFs, belong to 2D defects in 4H-SiC. Frank-type SFs are formed by adding or removing a Si-C bilayer, which are usually formed at the initial growth stage of 4H-SiC single crystals as a result of polymorph instability.[103] Shockley-type stacking faults (SSFs) associated with the Si-core and C-core partial dislocations are derived from the decomposition of BPDs.[104,105] Upon hole injection into the voltage-blocking layer of 4H-SiC bipolar devices, the slip of the Si-core partial dislocation gives rise to the expansion of the SSF, which decreases the forward voltage and increases the leakage current.[106–108] This is the so-called bipolar degradation induced by the expansion of SSFs.[109] Therefore, extremely long minority-carrier lifetime in the voltage-blocking layer is detrimental from the point of view of avoiding bipolar degradation. According to the stacking orders of SiC bilayers, SFs in 4H-SiC can also be distinguished by the Zhdanov's notation. Each type of SF has its characteristic luminescence, which facilitates the detection of stacking faults by photoluminescence, electroluminescence, or cathode luminescence measurements.[110–113]

From the point of view of restraining the expansion of SSF and enhancing the reliabilities of bipolar devices based on 4H-SiC, the minority (hole) carrier lifetime should not be extremely long in the lightly N-doped voltage-blocking 4H-SiC layer because the expansion of SSF is initiated by the injection of holes. In this case, the limitation of the carrier lifetime of holes can be restricted by inserting a minority-carrier recombination layer in the voltage-blocking layer of the 4H-SiC bipolar devices. The codoping of N with VAN and B has been shown to be capable of reducing the minority-carrier lifetime of 4H-SiC.[114,115] According to the electronic structures of native defects and impurities, V_C, Ti, and Fe are potential candidates to reduce the minority-carrier lifetime of 4H-SiC. Therefore, it is desirable to design a Si-rich condition to increase the V_C concentration and codoping N with minority-carrier lifetime killing impurities for the homoepitaxy of the minority-carrier recombination layer in the voltage-blocking layer of 4H-SiC bipolar devices.

Since the expansion of SSF is accompanied by the slip of the Si-core partial dislocation of a decomposed BPD, pinning the Si-core partial dislocation also holds promise in restraining the expansion of SSF in 4H-SiC. Substituting Si by isovalent impurities with larger atomic size is promising for pinning the Si-core partial dislocation and restraining SSF. A potential dopant is germanium (Ge), which does not change the electronic conductivity of 4H-SiC. By substituting Si,[116] the activation energy for the slip of Ge-core partial dislocations is higher than that of Si-core partial dislocations. This prevents the Si-core partial dislocation consisting a BPD from slipping, avoiding the formation and expansion of SSF during the service of 4H-SiC bipolar devices.

D. Three-dimensional defects

Three-dimensional (3D) defects including carbon inclusions, secondary polymorphs, micropipes, downfalls, carrot defects, and triangular defects are device-killing defects in 4H-SiC.[66] By optimizing growth conditions, the elimination of 3D defects is critical for the single-crystal growth and homoepitaxy of high-quality 4H-SiC.[26]

IV. OUTLOOK

The investigation on impurities and defects has enabled the impressive progress of 4H-SiC technologies. By analyzing recent advances and potential impurity engineering and defect engineering in 4H-SiC, we state that the following problems need to be addressed before the full potential of 4H-SiC is realized.

(1) Pushing forward the application of 4H-SiC in high-power and high-frequency electronics. The development of 4H-SiC in high-power electronics mainly concerns the optimization of the performance and reliability of 4H-SiC based medium- and high-voltage power devices as well as deepening the application of 4H-SiC in ultra-high-power electronics. The optimization of the performance and reliability of 4H-SiC based medium- and high-voltage power devices relies on both the point-defect engineering that improves the carrier lifetime and the dislocation control in 4H-SiC. The point-defect engineering focuses on the improvement of carrier lifetime in 4H-SiC. Reducing the concentration of V_C can be realized by designing C-rich growth conditions during the single-crystal growth and homoepitaxy of 4H-SiC. Furthermore, non-thermodynamic equilibrium post-growth treatments also need to be designed to eliminate detrimental defect states of V_C, which is capable of increasing the minority-carrier lifetime and ensuring uniform distribution of color centers in 4H-SiC. The dislocation control in 4H-SiC includes reducing the dislocation density and restraining SSFs from expansion. The design of buffer layers during the PVT- and CVD-growth of 4H-SiC to promote the conversion of TDs to basal plane defects is attractive to decrease the total dislocation density in commercialized 4H-SiC, which will significantly enhance the performance and reliability of 4H-SiC devices. In order to avoid the degradation of 4H-SiC based bipolar devices originating from the expansion of SSFs upon minority carrier injection, the codoping or Si-rich growth condition is critical to the epitaxy of the minority-carrier recombination layer for the voltage-blocking layer of the 4H-SiC bipolar devices. Meanwhile, the pinning of Si-core partial dislocations is also desired to push the commercialization of 4H-SiC bipolar devices and the use of 4H-SiC in ultra-high-power electronics. *p*-Type doping is one of the most important bottlenecks hindering the application of 4H-SiC in ultra-high-power electronics. The theory of improving the *p*-type doping of 4H-SiC has been established. Experimental efforts such as the codoping and compensation-defect elimination are highly desired to reduce

the resistivity of *p*-type 4H-SiC and explore the application of 4H-SiC in ultra-high-power electronics.

(2) Exploring the full potential of 4H-SiC in quantum technologies, photoconductive switches, radiation/optical detectors, and two-dimensional-material sciences. High-performance bipolar doping and defect control are the basis of broadening the application of 4H-SiC in quantum technologies, photoconductive switches, radiation/optical detectors, and 2D-material sciences. Reducing the unintentional induced point-defect concentration and dislocation density is critical to guaranteeing the optical fine structure of quantum emitters and maintaining stable spin coherence of optically active qubits. Furthermore, dislocation engineering that manipulates the configurations and electronic structures of screw dislocations is attractive to broaden the application of 4H-SiC in quantum technologies.

ACKNOWLEDGMENTS

This work was supported by the Natural Science Foundation of China (Grant Nos. 62274143 and 62204216), "Pioneer" and "Leading Goose" R&D Program of Zhejiang (Grant Nos. 2022C01021 and 2023C01010), and the Leading Innovative and Entrepreneur Team Introduction Program of Hangzhou (No. TD2022012). Partial support was provided by the Fundamental Research Funds for the Central Universities (Grant No. 226-2022-00200) and the Natural Science Foundation of China for Innovative Research Groups (Grant No. 61721005).

AUTHOR DECLARATIONS

Conflict of Interest

The authors have no conflicts to disclose.

Author Contributions

Rong Wang: Conceptualization (equal); Funding acquisition (equal); Writing – original draft (equal); Writing – review & editing (equal). **Yuanchao Huang:** Writing – review & editing (equal). **Deren Yang:** Conceptualization (equal); Funding acquisition (equal); Resources (equal); Writing – review & editing (equal). **Xiaodong Pi:** Conceptualization (equal); Funding acquisition (equal); Resources (equal); Writing – review & editing (equal).

DATA AVAILABILITY

The data that support the findings of this study are available from the corresponding authors upon reasonable request.

REFERENCES

[1]T. Kimoto and J. A. Cooper, *Fundamentals of Silicon Carbide Technology: Growth, Characterization, Devices, and Applications* (Wiley, 2014).
[2]P. Wellmann, N. Ohtoni, and R. Rupp, *Wide Bandgap Semiconductors for Power Electronics Materials, Devices, Applications* (Wiley, 2021).
[3]Q. Li, J. F. Wang, F. F. Yan, J. Y. Zhou, H. F. Wang, H. Liu, L. P. Guo, X. Zhou, A. Gali, Z. H. Liu, and Z. Q. Wang, Natl. Sci. Rev. **9**, nwab122 (2022).
[4]N. T. Son, C. P. Anderson, A. Bourassa, K. C. Miao, C. Babin, M. Widmann, M. Niethammer, J. U. Hassan, N. Morioka, I. G. Ivanov, F. Kaiser, J. Wrachtrup, and D. D. Awschalom, Appl. Phys. Lett. **116**, 190501 (2020).
[5]M. Suproniuk, P. Kamiński, R. Kozłowski, M. Pawłowski, and M. Wierzbowski, Opto-Electron. Rev. **25**, 171–180 (2017).
[6]I. Capan, Electronics **11**, 532 (2022).
[7]M. Mazzillo, G. Condorelli, M. E. Castagna, G. Catania, A. Sciuto, F. Roccaforte, and V. Raineri, IEEE Photonics Technol. Lett. **21**, 1782–1784 (2009).
[8]Y. Liu, Y. J. Fang, D. R. Yang, X. D. Pi, and P. J. Wang, J. Phys: Condens. Matter. **34**, 183001 (2022).
[9]Y. Matsushita, S. Furuya, and A. Oshiyama, Phys. Rev. Lett. **108**, 246404 (2012).
[10]S. Dimitrijev and P. Jamet, Microelectron. Reliab. **43**, 225–233 (2003).
[11]A. Alkauskas, M. D. McCluskey, and C. G. Van de Walle, J. Appl. Phys. **119**, 181101 (2016).
[12]H.-X. Deng, R. Cao, and S.-H. Wei, Sci. China: Phys., Mech. Astron. **64**, 237301 (2021).
[13]C. Freysoldt, B. Grabowski, T. Hickel, J. Neugebauer, G. Kresse, A. Janotti, and Ch. G. Van de Walle, Rev. Mod. Phys. **86**, 253 (2014).
[14]T. Kimoto, H. Niwa, T. Okuda, E. Saito, Y. Zhao, S. Asada, and J. Suda, J. Phys. D: Appl. Phys. **51**, 363001 (2018).
[15]J. J. Li, G. Yang, X. S. Liu, H. Luo, L. B. Xu, Y. Q. Zhang, C. Cui, X. D. Pi, D. R. Yang, and R. Wang, J. Phys. D: Appl. Phys. **55**, 463001 (2022).
[16]D. Segev and S.-H. Wei, Phys. Rev. Lett. **91**, 126406 (2003).
[17]R. Wang, X. D. Tong, J. X. Xu, S. Y. Zhang, P. H. Zheng, F. X. Chen, and W. Tan, Phys. Rev. Appl. **11**, 054021 (2019).
[18]X. F. Cai, J.-W. Luo, S.-S. Li, S.-H. Wei, and H.-X. Deng, Phys. Rev. B **106**, 214102 (2022).
[19]J.-H. Yang, J.-S. Park, J. Kang, W. Metzger, T. Barnes, and S.-H. Wei, Phys. Rev. B **90**, 245202 (2014).
[20]R. Wang, J. X. Xu, S. Y. Zhang, Z. Cheng, L. Zhang, P. H. Zheng, F. X. Chen, X. D. Tong, Y. Zhang, and W. Tan, Appl. Phys. Lett. **115**, 143504 (2019).
[21]X. She, A. Q. Huang, O. Lucia, and B. Ozpineci, IEEE Trans. Ind. Electron. **64**, 8193 (2017).
[22]O. Madelung, *Semiconductors: Data Handbook* (Springer, 2004).
[23]M. Ikeda, H. Matsunami, and T. Tanaka, Phys. Rev. B **22**, 2842–2854 (1980).
[24]X. L. Yan, P. Li, L. Kang, S.-H. Wei, and B. Huang, J. Appl. Phys. **127**, 085702 (2020).
[25]Y. C. Huang, R. Wang, Y. Q. Zhang, D. R. Yang, and X. D. Pi, Chin. Phys. B **31**, 056108 (2022).
[26]T. Kimoto, Prog. Cryst. Growth Charact. Mater. **62**, 329 (2016).
[27]L. Lu, H. Zhang, X. Wu, J. Shi, and Y.-Y. Sun, Chin. Phys. B **30**, 096806 (2021).
[28]I. G. Ivanov, B. Magnusson, and E. Janzén, Phys. Rev. B **67**, 165211 (2003).
[29]Y. C. Huang, R. Wang, Y. X. Qian, Y. Q. Zhang, D. R. Yang, and X. D. Pi, Chin. Phys. B **31**, 046104 (2022).
[30]C. Darmody and N. Goldsman, J. Appl. Phys. **126**, 145701 (2019).
[31]H. Matsuura, A. Takeshita, T. Imamura, K. Takano, K. Okuda, A. Hidaka, S. Y. Ji, K. Eto, K. Kojima, T. Kato, S. Yoshida, and H. Okumura, Appl. Phys. Express **11**, 101302 (2018).
[32]V. J. B. Torres, I. Capan, and J. Coutinho, Phys. Rev. B **106**, 224112 (2022).
[33]Y. Negoro, T. Kimoto, H. Matsunami, and G. Pensl, Jpn. J. Appl. Phys., Part 1 **46**, 5053 (2007).
[34]U. Forsberg, Ö. Danielsson, A. Henry, M. K. Linnarsson, and E. Janzén, J. Cryst. Growth **253**, 340 (2003).
[35]Y. C. Huang, R. Wang, Y. Q. Zhang, D. R. Yang, and X. D. Pi, J. Appl. Phys. **131**, 185703 (2022).
[36]H. M. Ayedh, A. Hallén, and B. G. Svensson, J. Appl. Phys. **118**, 175701 (2015).
[37]J. R. Jenny, D. P. Malta, V. F. Tsvetkov, M. K. Das, H. McD. Hobgood, C. H. Carter, Jr., R. J. Kumar, J. M. Borrego, R. J. Gutmann, and R. Aavikko, J. Appl. Phys. **100**, 113710 (2006).
[38]S. H. Lee, M. F. Bhopal, D. W. Lee, and S. H. Lee, Mater. Sci. Semicond. Process. **79**, 66 (2018).
[39]D.-Y. Chen, A. Malmros, M. Thorsell, H. Hjelmgren, O. Kordina, J.-T. Chen, and N. Rorsman, IEEE Electron Device Lett. **41**, 828 (2020).
[40]M. A. Mannan, K. V. Nguyen, R. O. Pak, C. Oner, and K. C. Mandal, IEEE Trans. Nucl. Sci. **63**, 1083 (2016).

[41]W. V. M. Machado, J. F. Justo, and L. V. C. Assali, J. Appl. Phys. **118**, 045704 (2015).
[42]W. C. Mitchela, W. D. Mitchell, G. Landis, H. E. Smith, W. Lee, and M. E. Zvanut, J. Appl. Phys. **101**, 013707 (2007).
[43]W. T. Fu, L. N. Wang, B. Wang, X. Chu, T. Xun, and H. W. Yang, AIP Adv. **12**, 095121 (2022).
[44]N. Sghaier, J. M. Bluet, A. Souifi, G. Guillot, E. Morvan, and C. Brylinski, IEEE Trans. Electron Devices **50**, 297 (2003).
[45]J. R. Jenny, D. P. Malta, S. G. Müller, A. R. Powell, V. F. Tsvetkov, H. M. Hobgood, R. C. Glass, and C. H. Carter, J. Electron. Mater. **32**, 432 (2003).
[46]J. D. Blevins, IEEE Trans. Semicond. Manuf. **33**, 539 (2020).
[47]S. Doğan, A. Teke, D. Huang, H. Morkoç, C. B. Roberts, J. Parish, B. Ganguly, M. Smith, R. E. Myers, and S. E. Saddow, Appl. Phys. Lett. **82**, 3107–3109 (2003).
[48]S. Jiang, C. Song, L. Zhang, Y. Zhang, W. Huang, and H. Guo, IEEE Trans. Electron Devices **63**, 1582–1586 (2016).
[49]W. W. Han, W. Huang, S. Y. Zhuo, J. Xin, X. C. Liu, E. W. Shi, Y. F. Zhang, P. H. Cao, Y. T. Wang, H. Guo, and Y. M. Zhang, IEEE Electron Device Lett. **40**, 271–274 (2019).
[50]P. H. Cao, W. Huang, H. Guo, and Y. M. Zhang, IEEE Trans. Electron Devices **65**, 2047–2051 (2018).
[51]M. Atatüre, D. Englund, N. Vamivakas, S.-Y. Lee, and J. Wrachtrup, Nat. Rev. Mater. **3**, 38–51 (2018).
[52]G. Wolfowicz, C. P. Anderson, B. Diler, O. G. Poluektov, F. J. Heremans, and D. D. Awschalom, Sci. Adv. **6**, eaaz1192 (2020).
[53]Y. Zhu, B. Kovos, M. Onizhuk, D. Awschalom, and G. Galli, Phys. Rev. Mater. **5**, 074602 (2021).
[54]J. F. Wang, F. F. Yan, Q. Li, Z. H. Liu, H. Liu, G. P. Guo, L. P. Guo, X. Zhou, J. M. Cui, J. Wang, Z. Q. Zhou, X. Y. Xu, J. S. Xu, C. F. Li, and G. C. Guo, Phys. Rev. Lett. **124**, 223601 (2020).
[55]A. Csóré, H. J. Von Bardeleben, J. L. Cantin, and A. Gali, Phys. Rev. B **96**, 085204 (2017).
[56]S. A. Zargaleh, B. Eble, S. Hameau, J.-L. Cantin, L. Legrand, M. Bernard, F. Margaillan, J.-S. Lauret, J.-F. Roch, H. J. von Bardeleben, E. Rauls, U. Gerstmann, and F. Treussart, Phys. Rev. B **94**, 060102 (2016).
[57]L. Spindlberger, A. Csóré, G. Thiering, S. Putz, R. Karhu, J. Hassan, N. T. Son, T. Fromherz, A. Gali, and M. Trupke, Phys. Rev. Appl. **12**, 014015 (2019).
[58]W. F. Koehl, B. Diler, S. J. Whiteley, A. Bourassa, N. T. Son, E. Janzén, and D. D. Awschalom, Phys. Rev. B **95**, 035207 (2017).
[59]T. Bosma, G. J. J. Lof, C. M. Gilardoni, O. V. Zwier, F. Hendriks, B. Magnusson, A. Ellison, A. Gällström, I. G. Ivanov, N. T. Son, R. W. A. Havenith, and C. H. van der Wal, npj Quantum Inf. **4**, 48 (2018).
[60]A. Gällström, B. Magnusson, S. Leone, O. Kordina, N. T. Son, V. Ivády, A. Gali, I. A. Abrikosov, E. Janzén, and I. G. Ivanov, Phys. Rev. B **92**, 075207 (2015).
[61]V. Ivády, J. Davidsson, N. T. Son, T. Ohshima, I. A. Abrikosov, and A. Gali, Phys. Rev. B **96**, 161114 (2017).
[62]N. T. Son, D. Shafizadeh, T. Ohshima, and I. G. Ivanov, J. Appl. Phys. **132**, 025703 (2022).
[63]K. Szász, V. Ivády, I. A. Abrikosov, E. Janzén, M. Bockstedte, and A. Gali, Phys. Rev. B **91**, 121201 (2015).
[64]J. P. Doyle, M. K. Linnarsson, P. Pellegrino, N. Keskitalo, and B. G. Svensson, J. Appl. Phys. **84**, 1354 (1998).
[65]K. Danno, D. Nakamura, and T. Kimoto, Appl. Phys. Lett. **90**, 202109 (2007).
[66]T. Kimoto and H. Watanabe, Appl. Phys. Express **13**, 120101 (2020).
[67]P. B. Kleina and B. V. Shanabrook, Appl. Phys. Lett. **88**, 052110 (2006).
[68]N. T. Son, X. T. Trinh, L. S. Løvlie, B. G. Svensson, K. Kawahara, J. Suda, T. Kimoto, T. Umeda, J. Isoya, T. Makino, T. Ohshima, and E. Janzén, Phys. Rev. Lett. **109**, 187603 (2012).
[69]I. D. Booker, E. Janzén, N. T. Son, J. Hassan, P. Stenberg, and E. Ö. Sveinbjörnsson, J. Appl. Phys. **119**, 235703 (2016).
[70]L. S. Zhao, Y. D. Tang, Y. Bai, M. L. Qiu, Z. K. Wu, Y. Yang, C. Y. Yang, X. L. Tian, and X. Y. Liu, Electronics **11**, 1341 (2022).
[71]H. Bencherif, L. Dehimi, N. Athamena, F. Pezzimenti, M. L. Megherbi, and F. G. D. Corte, Silicon **13**, 3629 (2021).
[72]T. Kimoto, T. Hiyoshi, T. Hayashi, and J. Suda, J. Appl. Phys. **108**, 083721 (2010).
[73]A. Akturk, R. Wilkins, J. McGarrity, and B. Gersey, IEEE Trans. Nucl. Sci. **64**, 529 (2017).
[74]C. Hemmingsson, N. T. Son, O. Kordina, J. P. Bergman, and E. Janzén, J. Appl. Phys. **81**, 6155 (1997).
[75]K. Danno and T. Kimoto, J. Appl. Phys. **100**, 113728 (2006).
[76]J. S. Embley, J. S. Colton, K. G. Miller, M. A. Morris, M. Meehan, S. L. Crossen, B. D. Weaver, E. R. Glaser, and S. G. Carter, Phys. Rev. B **95**, 045206 (2017).
[77]I. Capan, T. Brodar, Y. Yamazaki, Y. Oki, T. Ohshima, Y. Chiba, Y. Hijikata, L. Snoj, and V. Radulović, Nucl. Instrum. Methods Phys. Res., Sect. B **478**, 224–228 (2020).
[78]I. Capan, T. Brodar, T. Makino, V. Radulovic, and L. Snoj, Crystals **11**, 1404 (2021).
[79]S. B. Orlinski, J. Schmidt, E. N. Mokhov, and P. G. Baranov, Phys. Rev. B **67**, 125207 (2003).
[80]H. Kaneko and T. Kimoto, Appl. Phys. Lett. **98**, 262106 (2011).
[81]L. Liu, J. F. Wang, X. D. Liu, H. A. Xu, J. M. Cui, Q. Li, J. Y. Zhou, W. X. Lin, Z. X. He, W. Xu, and Y. Wei, Nano Lett. **22**, 9943 (2022).
[82]W. X. Lin, F. F. Yan, Q. Li, J. F. Wang, Z. H. Hao, J. Y. Zhou, H. Li, L. X. You, J. S. Xu, C. F. Li, and G. C. Guo, Phys. Rev. B **104**, 125305 (2021).
[83]S. Yang, X. W. Liang, J. W. Cui, Q. W. Zheng, J. Sun, M. Liu, D. Zhang, H. N. Feng, X. F. Yu, C. F. Xiang, Y. D. Li, and Q. Guo, J. Semicond. **42**, 082802 (2021).
[84]P. Hazdra and J. Vobecký, Phys. Status Solidi A **216**, 1900312 (2019).
[85]P. Hazdra, S. Popelka, and A. Schöner, Mater. Sci. Forum **924**, 436 (2018).
[86]S. Ichikawa, K. Kawahara, J. Suda, and T. Kimoto, Appl. Phys. Express **5**, 101301 (2012).
[87]W. D. Gao, G. Yuang, Y. X. Qian, X. F. Han, C. Cui, X. D. Pi, D. R. Yang, and R. Wang, Front. Mater. **10**, 1022878 (2023).
[88]G. Feng, J. Suda, and T. Kimoto, J. Appl. Phys. **110**, 033525 (2011).
[89]H. Luo, J. J. Li, G. Yang, R. Z. Zhu, Y. Q. Zhang, R. Wang, D. R. Yang, and X. D. Pi, ACS Appl. Electron. Mater. **4**, 1678 (2022).
[90]L. Hu, H. Q. Huang, Z. F. Wang, W. Jiang, X. J. Ni, Y. N. Zhou, V. Zielasek, M. G. Lagally, B. Huang, and F. Liu, Phys. Rev. Lett. **121**, 066401 (2018).
[91]P. J. Wellmann, Semicond. Sci. Technol. **33**, 103001 (2018).
[92]T. Kimoto, K. Yamada, H. Niwa, and J. Suda, Energies **9**, 908 (2016).
[93]F. La Via, M. Camarda, and A. La Magna, Appl. Phys. Rev. **1**, 031301 (2014).
[94]D. Nakamura, I. Gunjishima, S. Yamaguchi, T. Ito, A. Okamoto, H. Kondo, S. Onda, and K. Takatori, Nature **430**, 1009–1012 (2004).
[95]T. Mitani, K. Eto, N. Komatsu, Y. Hayashi, H. Suo, and T. Kato, J. Cryst. Growth **568–569**, 126189 (2021).
[96]S. Harada, Y. Yamamoto, K. Seki, A. Horio, T. Mitsuhashi, M. Tagawa, and T. Ujihara, APL Mater. **1**, 022109 (2013).
[97]S. Harada, Y. Yamamoto, K. Seki, A. Horio, M. Tagawa, and T. Ujihara, Acta Mater. **81**, 284 (2014).
[98]J. J. Li, H. Luo, G. Yang, Y. Q. Zhang, X. D. Pi, D. R. Yang, and R. Wang, Phys. Rev. Appl. **17**, 054011 (2022).
[99]X. S. Liu, J. R. Zhang, B. J. Xu, Y. H. Lu, Y. Q. Zhang, R. Wang, D. Yang, and X. D. Pi, Appl. Phys. Lett. **120**, 052105 (2022).
[100]X. S. Liu, R. Wang, J. Zhang, Y. H. Lu, Y. Q. Zhang, D. R. Yang, and X. D. Pi, J. Appl. Phys. D: Appl. Phys. **55**, 334002 (2022).
[101]R. Wang, X. D. Tong, J. X. Xu, C. L. Dong, Z. Cheng, L. Zhang, S. Y. Zhang, P. H. Zheng, F.-X. Chen, Y. Zhang, and W. Tan, Phys. Rev. Appl. **14**, 024039 (2020).
[102]R. Wang, J. X. Xu, S. Y. Zhang, Y. Zhang, P. H. Zheng, Z. Cheng, L. Zhang, F.-X. Chen, X. D. Tong, Y. Zhang, and W. Tan, J. Mater. Chem. C **9**, 3177–3182 (2021).
[103]Q. Q. Shao, W. H. G, P. L. Chen, X. Zhang, R. H. Shen, H. Tian, X. D. Pi, D. R. Yang, and R. Wang, "Nucleation of treading dislocations in 4H-SiC during the initial growth of physical-vapor transport" (unpublished).
[104]A. Iijima, I. Kamata, H. Tsuchida, J. Suda, and T. Kimoto, Philos. Mag. **97**, 2736 (2017).
[105]J. D. Caldwell, A. Giles, D. Lepage, D. Carrier, K. Moumanis, B. A. Hull, R. E. Stahlbush, R. L. Myers-Ward, J. J. Dubowski, and M. Verhaegen, Appl. Phys. Lett. **102**, 242109 (2013).

[106]Y. Ishikawa, M. Sudo, Y. Z. Yao, Y. Sugawara, and M. Kato, J. Appl. Phys. **123**, 225101 (2018).
[107]A. Tanaka, H. Matsuhata, N. Kawabata, D. Mori, K. Inoue, M. Ryo, T. Fujimoto, and T. Tawara, J. Appl. Phys. **119**, 095711 (2016).
[108]A. Galeckas, J. Linnros, and P. Pirouz, Phys. Rev. Lett. **96**, 025502 (2006).
[109]Y. Bu, H. Yoshimoto, N. Watanabe, and A. Shima, J. Appl. Phys. **122**, 244504 (2017).
[110]B. Chen, T. Sekiguchi, T. Ohyanagi, H. Matsuhata, A. Kinoshita, and H. Okumura, Phys. Rev. B **81**, 233203 (2010).
[111]Y. Tokuda, I. Kamata, N. Hoshino, T. Kato, H. Okumura, T. Kimoto, and H. Tsuchida, J. Cryst. Growth **468**, 889 (2017).
[112]S. I. Maximenko, J. A. Freitas, Y. N. Picard, P. B. Klein, R. L. Myers-Ward, K. K. Lew, P. G. Muzykov, D. K. Gaskill, C. R. Eddy, and T. S. Sudarshan, Mater. Sci. Forum **645–648**, 211 (2010).
[113]N. Thierry-Jebali, C. Kawahara, T. Miyazawa, H. Tsuchida, and T. Kimoto, AIP Adv. **5**, 037121 (2015).
[114]K. Murata, T. Tawara, A. Yang, R. Takanashi, T. Miyazawa, and H. Tsuchida, J. Appl. Phys. **126**, 045711 (2019).
[115]A. Yang, K. Murata, T. Miyazawa, T. Tawara, and H. Tsuchida, J. Appl. Phys. **126**, 055103 (2019).
[116]G. Ferro, Crit. Rev. Solid State Mater. Sci. **47**, 520 (2022).